MATHEMATICAL MODELING AND COMPUTING, Vol. 12, No. 1, pp. 248–263 (2025)

Numerical simulation of bi-disperse polymer flow in complex geometries using Rolie–Double–Poly model within OpenFOAM software

Azahar A. A.[1], Oliver G. H.[2], Mark A. W.[3], Ramli N.[1]

[1]*School of Mathematical Sciences, University Sains Malaysia, 11800 USM, Penang, Malaysia*
[2]*School of Mathematics, University of Leeds, LS2 9JT, United Kingdom*
[3]*School of Computing, University of Leeds, LS2 9JT, United Kingdom*

(Received 19 November 2024; Revised 24 February 2025; Accepted 25 February 2025)

Modeling the behavior of bi-disperse, linearly entangled polymers blends using the Rolie–Double–Poly constitutive equation is essential for understanding the reliability of the model in simulating complex flow behaviors. This study examines the extensional response of polymer blends, particularly the stretching of chains under pure extensional flow along the centre-line in two flow geometries: hyperbolic contraction flow and cross-slot flow with hyperbolic corners. Coupled and uncoupled models were implemented within the OpenFOAM software via the `RheoTool` toolbox where the simulations use the `rheoFoam` solver to model incompressible viscoelastic fluid flow. The effect including the contraction lengths, blend composition of chain lengths, and chain coupling are the key factors in this studies. One significant results reveal that the Rolie–Double–Poly model more accurately captures the extensional behavior of polymer chains compared to the uncoupled model underscoring its potential applicability for more complex, polydisperse systems.

Keywords: *Rolie–Double–Poly; Rolie–Poly; hyperbolic contraction flow; cross–slot flow; OpenFOAM, RheoTool.*

2010 MSC: 76A05, 76A10, 76M12, 65M99, 76A99 **DOI:** 10.23939/mmc2025.01.248

1. Introduction

Understanding the behavior of polymeric fluids during processing is crucial for controlling their flow and optimizing processing parameters. This insight plays a vital role in achieving high-quality and consistent final products. However, a significant challenge in this field, particularly when using numerical simulations, is selecting an appropriate constitutive model that accurately predicts the flow behavior. These models must effectively represent the intricate molecular dynamics essential for computational fluid dynamics simulations.

Over time, the constitutive models describing viscoelasticity have evolved significantly from the basic Maxwell model [1], which described linear unentangled polymers using a simple spring and dashpot, to more advanced models that address the polydispersity of entangled polymer chains Boudara et al. [2] and not limited to linear polymer. Researchers used relevant theories to develop the models. For instance, a sophisticated GLaMM model [3] was derived based on the tube theory of de Gennes [4] and Doi and Edwards [5], to describe the monodisperse linear polymer melts. The comparison between the prediction made by the model has been verify experimentally for polyisoprene melts where the prediction of the model is align with the observed behavior of the monodisperse melts in nonlinear shear flows conditions [6]. The GLaMM model also has been used by other researchers for comparison with the experimental results [7–9]. Likhtman and Graham [10] simplify the GLaMM model to form Rolie–Poly model that retain the features of the GLaMM model so that it is amenable for computational fluid dynamics [11, 12]. Numerous research work utilizing this model to study the flow behavior under different conditions [13–16]. Although these models are effective for monodisperse polymer melts, it fails to capture the blends of different polymer chain lengths typically found in industrial grade

This research was funded by a grant from University Sains Malaysia (Short Term Grant 304.PMATHS.6315718).

polymer. The conventional way of defining polydispersity ignores the interactions between polymer chains that leads to inaccuracy of the prediction. The uncoupled model is based on the principle of linear superposition, is referred to as the multimode model. The stress of the multimode model is computed by summing the individual contribution of the polymer chains involved.

Due to the limitations in accurately describing polydispersity in existing multimode model, Boudara et al. [2] proposed a new model that effectively captures the polydispersity of polymers using a double reptation framework [17]. This approach accounts for the interactions between different polymer species, better mimicking real polymer behavior. The Rolie–Double–Poly (RDP) model defines stress contributions as the sum of the individual polymer species, incorporating entanglements specific to each species within the blend and their respective volume fractions. However, a key challenge of this model arises as the number of components in the blend increases, significantly complicating the computational process.

Geometrical flows are commonly used to study the viscoelastic response of the models considered. The abrupt 4:1 contraction geometry is one of the benchmark geometrical flows that has been used to study the viscoelastic response under complex flow, the mixture between shear near the wall and pure elongational flow at the centre–line. However, the disadvantage of the device is the formulation of the flow recirculation near the edges of the upstream corner before the fluid accelerating through the constriction region under fast flow. Understanding the extensional response in this configuration is quite challenging due to abrupt geometrical changes which trigger the intense elongational flow as the fluid moves through the downstream. This implies a uniform extension-rate fail to be obtained [18]. In 1978, Cogswell [19] investigated various converging geometries to examine the fluid response under elongational flow and found that a uniform extension-rate was observed within the converging region for the hyperbolic contraction configuration. This discovery suggests that the hyperbolic contraction profile is an effective alternative device for measuring extensional viscosity, aiding in the prediction of extensional viscosity within the contracting region. Consequently, many researchers have utilized this device to study the elongational flow behavior of viscoelastic models [20] and commercial polymers [21, 22].

Although the hyperbolic contraction configuration is effective for measuring extensional viscosity, the amount of strain experienced by the fluid during stretching flow may be limited compared to other configurations. The cross-slot geometry is another useful setup for studying how viscoelastic fluids respond to strong stretching flow. It helps provide a clearer picture of the fluid's behaviors under intense elongational flow. In 2014, Cruz et al. [23] suggested the cross-slot device as a new benchmark flow for viscoelastic fluids. Many researchers have utilized cross-slot device to investigate various aspects of fluid behavior, demonstrating its versatility in studying different phenomena [24–28].

The RDP constitutive equation [2], a recently introduced model, effectively describes polydispersity. However, limited research has explored its application, leaving a gap in understanding. This paper aims to fill this gap by investigating the behavior of the bi-disperse model in complex geometrical flows, with a focus on its extensional behavior. The study compares this model to traditional methods of defining bi-dispersity, particularly in terms of elastic response under pure elongational flow. Specifically, the paper examines the behavior of bi-disperse blends described by the RDP model in one-dimensional 4:1 hyperbolic contraction flow and two-dimensional cross-slot flow with hyperbolic corners.

2. The Rolie–Poly and Rolie–Double–Poly constitutive equation

Rolie–Poly model was originally proposed by Likhtman and Graham [10] delineates shear-thinning fluid based on molecular and tube theory [5] and a simplification of the GLaMM model that characterizes the monodisperse linear entangled polymer [3]. The polymeric stress, σ is defined based on conformation stress, $\mathbf{A}$ as $\sigma = G\mathbf{A}$, where G is the elastic modulus and for $\mathbf{A}$ for Rolie–Poly model is described as

$$\overset{\triangledown}{\boldsymbol{A}} = \underbrace{-\tfrac{1}{\tau_d}(\mathbf{A}-\mathbf{I})}_{\text{Reptation}} \underbrace{-\tfrac{2}{\tau_s}(1-\lambda^{-1})\left[\mathbf{A}+\beta^*\lambda^{2\delta}(\mathbf{A}-\mathbf{I})\right]}_{\text{Retraction and CCR}}, \tag{1}$$

where $\overset{\triangledown}{\boldsymbol{A}}$ is the upper-convected time derivative, β^* is convective constraint release, (CCR) coefficient, $\delta = -0.5$ is the fitting parameter and $\lambda = \sqrt{\frac{\mathrm{tr}\,(\mathbf{A})}{3}}$ is the molecular stretch of the polymer chain, τ_d is the reptation relaxation time and τ_s is the stretch relaxation time. As for the multimode Rolie–Poly (mRP) model, the total polymeric stress is based on the summation of the stresses from the individual mode and neglects the interaction of the polymeric chains involved in the blends. The total polymeric stress of the mRP model is calculated as $\boldsymbol{\sigma} = \sum_{M=1}^{N} \boldsymbol{\sigma}_M$, where $\boldsymbol{\sigma}_M$ is the polymeric stress of mode M and N is the total number of modes. Note that, each mode has a different elastic modulus and relaxation time. For comparison purposes between mRP and RDP, the parameters considered are calculated based on the same linear viscoleastic envelope.

In this work, the bi-disperse blends is considered involving two different molecular weights, the short chain, S and the long chain, L from the same polymer with respective to ensure the proportionality of the elastic modulus to volume fraction, ϕ_S and ϕ_L.

The original total polymeric stress of RDP model defined by Boudara et al. [2] involving finite extensibility function and assume as one in this work. The stress is then defined as

$$\boldsymbol{\sigma} = G(\phi_S \boldsymbol{A}_S) + (\phi_L \boldsymbol{A}_L), \tag{2}$$

where $\mathbf{A}_S$ and $\mathbf{A}_L$ denote the mean conformation stress tensors from the interactions of the short and long chains, with the respective stretches defined as $\lambda_S = \sqrt{\mathrm{tr}\,\mathbf{A}_S/3}$ and $\lambda_L = \sqrt{\mathrm{tr}\,\mathbf{A}_L/3}$. The mean conformation tensors are given as

$$\boldsymbol{A}_S = \phi_L \boldsymbol{A}_{SL} + \phi_S \boldsymbol{A}_{SS}, \tag{3}$$

$$\boldsymbol{A}_L = \phi_S \boldsymbol{A}_{LL} + \phi_S \boldsymbol{A}_{LS}, \tag{4}$$

where $\mathbf{A}_{IJ}$ represents the conformation of type I chains resulting from entanglements with type J chains. In general, each tensor can be described as

$$\overset{\triangledown}{\boldsymbol{A}} = \underbrace{-\tfrac{1}{\tau_{d,I}}(\boldsymbol{A}_{IJ} - \boldsymbol{I})}_{\text{Reptation}} \underbrace{-\tfrac{2}{\tau_{s,I}}(1-\lambda_I^{-1})\boldsymbol{A}_{IJ}}_{\text{Retraction}} \underbrace{-\tfrac{\beta_{th}}{\tau_{d,J}}(\boldsymbol{A}_{IJ} - \boldsymbol{I})}_{\text{Thermal contraint release}} \underbrace{-\tfrac{2\beta^*\lambda_I^{2\delta}}{\tau_{s,I}}(1-\lambda_J^{-1})(\boldsymbol{A}_{IJ} - \boldsymbol{I})}_{\text{Convective constraint release}}. \tag{5}$$

The coupling effect between the chain interaction is examined using RDP model with 5% long chain having the orientation relation time, $\tau_{d,L} = 10$ and stretch relaxation time, $\tau_{s,L} = 0.2$ in arbitrary units blended with 95% of short chain with $\tau_{d,S} = 0.1$ and $\tau_{s,S} = 0.05$. The results presented in this paper considering the parameters with respective values and $\beta^* = 0$ and $\beta_{th} = 1$.

Utilizing a two-mode RP model, which is based on the contributions from the short and long chains is insufficient to produce comparable results for comparison purposes. This effect is compared with the mRP model for the uncoupled version of bi-dispersity. To achieve comparable results that match the linear rheology as the RDP, a three-mode RP is selected to study the coupling effect. Therefore, the corresponding relaxation times for the three-mode RP model are defined as

$$\tau_{d,1} = \tfrac{\tau_{d,L}}{2}, \qquad \tau_{d,2} = \left(\tfrac{1}{\tau_{d,L}} + \tfrac{1}{\tau_{d,S}}\right)^{-1}, \qquad \tau_{d,3} = \tfrac{\tau_{d,S}}{2} \tag{6}$$

and the stretch relaxation times for the modes are given as

$$\tau_{s,1} = \tau_{s,L}, \qquad \tau_{s,2} = 2\left(\tfrac{1}{\tau_{s,L}} + \tfrac{1}{\tau_{s,S}}\right)^{-1}, \qquad \tau_{s,S} = \tau_{s,S}, \tag{7}$$

with respective moduli as $G_1 = G\phi_L^2$, $G_2 = 2G\phi_L\phi_S$ and $G_3 = G\phi_S^2$. These parameters set for three-mode RP model give the same predictions as the RDP model in the linear viscoelastic limit. The first mode can be viewed as representing the long-long configuration, the second mode as representing the configuration made by long-short and short-long and the third mode with short-short configuration. One significant difference between the RDP and mRP models is that the ability of the model to capture strain hardening below the extension-rate below $1/\tau_{s,L}$ due to the enhanced stretch relaxation [29] of the polymer chain with higher molecular weight of the polymer chain in the blends. This affect the increment of the effective stretch relaxation time of the long chain and the phenomenon has been investigated and confirmed this behavior experimentally [30] and explained theoretically [29].

3. OpenFOAM simulations

The OpenFOAM software [31] is used in this study to simulate the results presented. This open-source software, written in the high-level C++ is based on finite-volume solver developed to solve various computational fluid dynamic problems. The viscoelastic solver, `viscoelasticFluidFoam` was first introduced by Favero et al. [32] within the `foam-extend` library. However, due to stability issue under certain conditions, Pimenta and Alves [33] developed a more robust solver called `rheoFoam`, available in a `RheoTool` toolbox. This solver is specifically used for simulating single-phase, transient, incompressible flows of the Generalized Newtonian and viscoelastic fluids.

`RheoFoam` solver utilizes the SIMPLEC algorithm [34] for the pressure-velocity coupling and employs the CUBISTA scheme for discretizing the convective terms which ensures second-order accuracy in both time and space. Pimenta and Alves [33] validated the `rheoFoam` solver by comparing the performance on the Oldroyd-B flow through an abrupt 4:1 contraction with their in-house finite volume code for Deborah numbers up to 12. The study found good agreement between the two approaches demonstrating the accuracy and stability of the solver under challenging flow conditions. This comparison supports the reliability of the `rheoFoam` code for modeling complex viscoelastic flows.

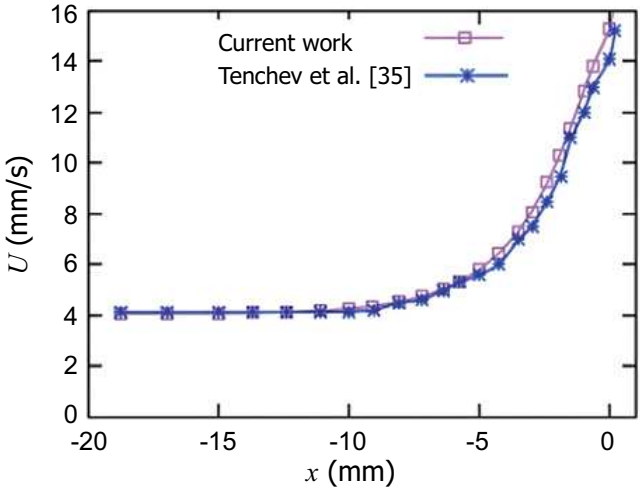

Fig. 1. Comparison for velocity distribution at the centreline towards the contracting region between `rheoFoam` (current work) and the finite element solver [35].

The `RheoTool` toolbox has been extended to include the three-mode mRP and RDP models within the software. The implementation of the mRP model was validated against the finite element algorithm developed by Tenchev et al. [35] through comparisons of results from 4:1 planar contraction flow simulations for the commercial-grade polystyrene, PS2 as shown in Figure 1.

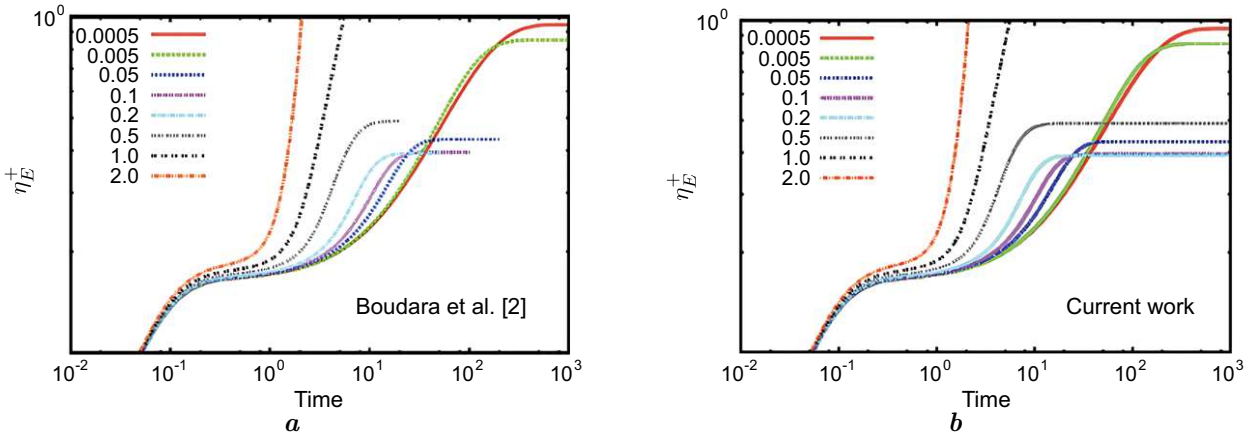

Fig. 2. Validation of the implemented RDP model by comparing the transient uniaxial extensional viscosity from the published results by (***a***) Boudara et al. [2] (LHS) with (***b***) current work (RHS) for 5% long chain blend with 95% short chain having relaxation times of $\lambda_{D,L} = 200$, $\lambda_{R,L} = 1.0$, $\lambda_{D,S} = 0.1$, $\lambda_{R,S} = 0.01$).

The validation of the implemented RDP model was conducted by comparing the transient uniaxial extensional calculation given by Boudara et al. [2]. Figure 2 shows the agreement between the results obtained using `rheoTestFoam` solver shown in Figure 2*b* and the results from Figure 2*a* available in [2]. This demonstrates the reliability of the RDP implementation within `RheoTool` toolbox.

4. Result

4.1. Hyperbolic contraction flow

The abrupt contraction flow is commonly used as the benchmark geometrical flows to study the extensional response of the viscoelastic fluid flow flowing in one-dimensional. The strain-rate history of the stretching flow through the constriction is depends on the rheological characteristics of the fluid considered that affect the formation of the fluid pattern in the upstream region especially near the vertex of the converging region.

One of the disadvantages of abrupt contraction device is the formulation of the flow recirculation near the edges of the corner before the fluid flowing through the constriction with high rates depending on the contraction ratio. The hyperbolic contraction geometry as an alternative device can be used to study the extensional behavior of the fluid at the centre-line within the contracting region. This is because, hyperbolic contraction geometry can be considered as a tool to generate a constant extension-rate at the centre-line that can be used to measure the extensional viscosity which an important stretching fluid property [19].

In this study, we examine a 4:1 planar hyperbolic contraction to analyze the behavior of fluid flow under controlled extensional and shear conditions. The flow transitions from a wider upstream inlet channel to a narrower downstream outlet channel, creating a contraction ratio of 4:1. To achieve a smooth flow profile through the contraction, a hyperbolic design is implemented, which ensures a gradual decrease in cross-sectional area within the constriction region. This design generates a controlled acceleration of fluid as it enters the contraction, resulting in a uniform velocity gradient along the centre-line of the geometry and promoting a constant extension-rate in the central flow region. Close to the channel walls, shear stress dominates, while a combination of shear and extensional stresses occurs across the contraction, producing a complex flow profile. This hyperbolic contraction geometry is particularly effective for studying the extensional response of fluids, making it valuable in experimental investigations involving viscoelastic and other complex fluids.

As a consequence of the symmetry with the upstream and downstream at the centre-line of the geometry, only half of geometry with the contraction ratio of the upstream to downstream, 4:1 is considered as shown in Figure 3. This reduced the computational cost during the simulation,

$$H(x) = \begin{cases} H_0, & x \leqslant 0, \\ \frac{H_0 L}{L+(H_0/H_1-1)x}, & 0 < x < L, \\ H_1, & x \geqslant L \end{cases}$$

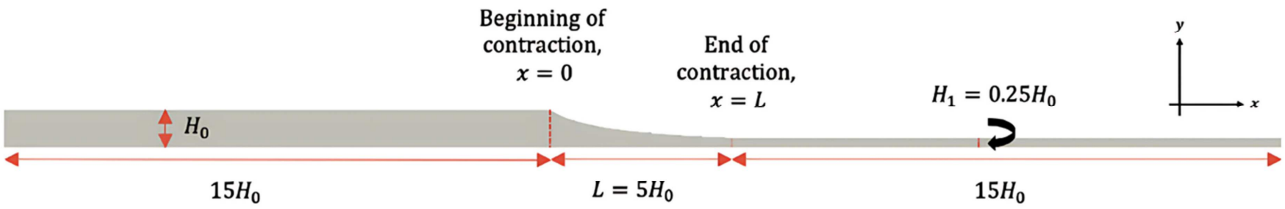

Fig. 3. The computational domain for the upper half of the hyperbolic contraction used for simulating the HCF using the RDP model with symmetry imposed on $y = 0$. The contraction length shown by the schematic is $L = 5$.

Pressure ramping protocol is used to evolve the flow with the smooth onset at the inlet in the upstream with no slip boundary condition set up at the wall and `linearExtrapolation` utility as a boundary condition to extrapolate the stress at the wall. The following pressure formula is used in the simulation, $P = \alpha(1 - e^{-\beta t})$, where α is the target pressure drop value and β is set to 1 and t is time. It is worth noting that the pressure ramping protocol had no effect to the prediction of the final steady-state.

The effect of the contraction length, the coupling effect between the Rolie–Double–Poly (RDP) and multimode Rolie–Poly (mRP) and the effect of blend composition are studied to understand the

behavior of the geometrical changes towards the extensional components, the consideration of the interaction between the polymer chains described by the RDP model through coupling effect and the existence of different volume fractions for the long and the short chains in the blend.

4.1.1. Effect of contraction length

In this paper, two contraction lengths, $L = 1$ and $L = 5$ are considered to observe to generate a constant extension-rate within the contracting region along the centre-line. A good meshing strategy is required especially when dealing with the short contracting region to avoid the high skewness issue that complicate computations during simulations. Figure 4 illustrates the generated extension-rate along the centre-line for contraction length $L = 1$ and $L = 5$ at an upstream volumetric flow-rate, (VFR) of approximately, VFR ≈ 3.12. The results shows that the shorter contraction length ($L = 1$) generated higher but non-uniform extension-rate comparing to longer extension-rate. The contraction length, $L = 5$ is considered long enough to generate high extension-rate and preserve the extensional flow characteristics. At the end of the contraction that is the beginning of the downstream channel, negatives extension-rate are observed due to elastic recoil.

A hyperbolic contraction length of $L = 5$ in this study is considered optimal, as it achieves a uniform and sufficient extension-rate along the centre–line. However, extending the contraction length beyond reduces the extension–rate and for sufficient long hyperbolic contraction length leads to highly shear–dominated flow near the walls, which interferes the formation of the purely elongational flow at the centre-line of the geometry. Therefore, selecting an optimal contraction length is essential to investigate the elastic behavior of the polymeric model without inducing elastic instabilities or shear-dominated flow. This optimal length should enhance the quality of extensional flow and allow a better understanding of the stretching behavior of the polymeric model considered. Another significant geometric factor influencing extensional flow in hyperbolic contraction geometry is the contraction ratio. For a given extension-rate and contraction length, a higher contraction ratio is believed to give greater extensional strain due to the increased residence time within the contraction region.

As a consequence of the extension-rate generated in Figure 4, the stretches for both the long-long chain entanglement, or so called the fat tube and the thin tube formed from both short and long chain entanglement are depicted in Figure 5. The design of the shorter contraction length ($L = 1$) of the geometry allow the flow to experience intense elongational flow through the constriction region that generates higher stretch comparing to longer contraction length ($L = 5$). The abrupt changes of the geometry downstream generates higher extension-rate that spikes the stretch. However, for the longer contraction length ($L = 5$), the changes of the geometry is smoother allowing the flow to accelerate through the converging region gradually and create uniform extension-rate along the centre-line within the converging region.

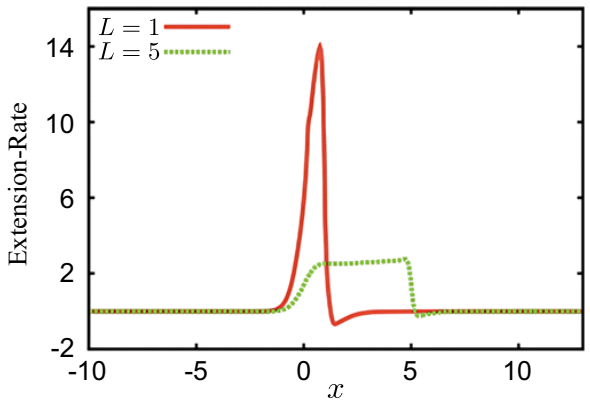

Fig. 4. The extension-rate of the bi-disperse RDP model with different contraction lengths of the hyperbolic contraction flow.

The contraction length within the constricting region is an important aspect of the geometry to ensure the uniform extension-rate can be achieved. However, the geometrical flow behavior is a complex interplay between shear and elongational response. Therefore, to prevent the shear effects from dominating the flow especially away from the centre-line, a balance must be achieved between having sufficiently long contraction region contraction with sufficiently high extension-rate that gives high enough extension-rate. This compromise helps to preserve the elongational flow characteristics without being overshadowed by shear.

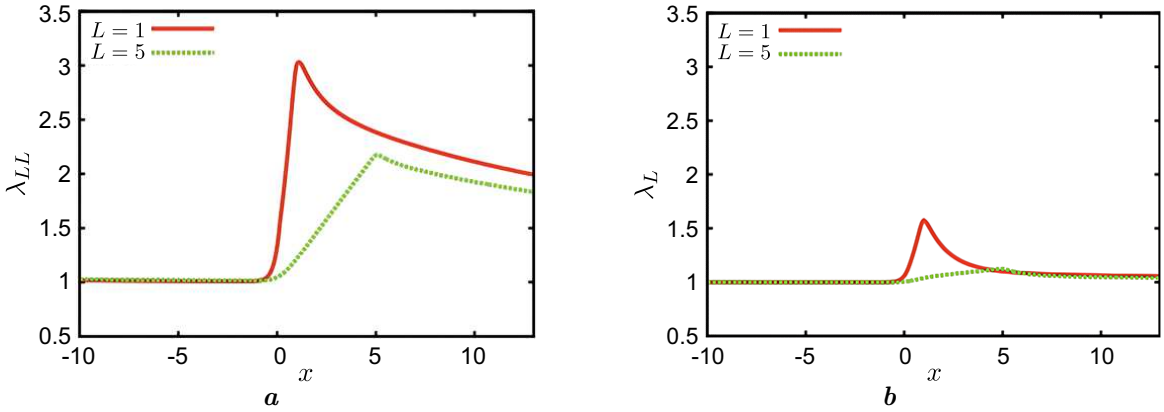

Fig. 5. Centre-line plot for different contraction length, $L = 1$ and $L = 5$ of the hyperbolic contraction flow with VFR ≈ 3.12 predicted by bi-disperse RDP model. (***a***) Left-hand figure shows the fat-tube stretches. (***b***) Right-hand figure shows the thin tube stretches.

4.1.2. Coupling effect

Table 1. The respective parameters for the three-mode mRP model based on the RDP parameters.

Parameters	Mode 1	Mode 2	Mode 3
$\eta_{p,j}$	0.0125	0.009406	0.045125
$\tau_{d,j}$	5.0	0.0990099	0.05
$\tau_{p,j}$	0.2	0.08	0.05

Investigating the effect of the interaction between the polymer chains in blends is crucial to ensure that numerical predictions accurately reflect the real polymer behavior. This section compares two models, the mRP model that neglects the chains interaction and RDP model that considers the interaction between the chain involved. Both models describes the bi-dispersity with the same prediction in the linear viscoelastic limit. The equivalent parameters for 3 mode mRP model based on RDP parameter are displayed in Table 1, where j in Table 1 is $j = 1, 2, 3$.

It is worth noting that the value of the $\tau_{d,j}$ and $\tau_{s,j}$ obtained in Table 1 is calculated using Eqs. (6) and (7). The viscosity for each mode is defined as follow

$$\eta_{p,1} = \frac{G\phi_L^2\tau_{d,L}}{2} = \eta_{p,L}\frac{\phi_L}{2}, \tag{8}$$

$$\eta_{p,2} = 2G\phi_L\phi_S\left(\frac{1}{\tau_{d,L}} + \frac{1}{\tau_{d,S}}\right)^{-1} = 2\eta_{p,L}\frac{\phi_S}{\tau_{d,L}}\left(\frac{1}{\tau_{d,L}} + \frac{1}{\tau_{d,S}}\right)^{-1}, \tag{9}$$

$$\eta_{p,3} = \frac{G\phi_S^2\tau_{d,S}}{2} = \eta_{p,S}\frac{\phi_S}{2}. \tag{10}$$

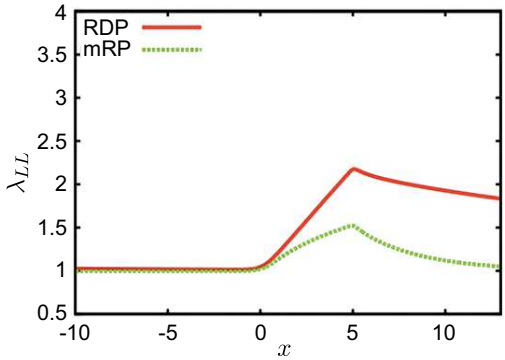

Fig. 6. Centre–line plot between RDP and mRP for the 4:1 hyperbolic contraction flow, with $L = 5$ for the stretch for the fat tube composed only of L-chains, $\lambda_{LL} = \sqrt{\mathrm{tr}\, A_{LL}/3}$ predicted by the (coupled) RDP model compare to (uncoupled) mRP model.

Figure 6 shows the comparison between the stretch for the long-long chain component. In mRP, the stretch of the long-long chain configuration is represented by the first mode of the model. From the figure, it is observed that the prediction of the fat tube stretch made by the RDP model flowing in 4:1 contraction ratio is approximately $\lambda_{LL} \approx 2.17$ which is about 1.4 times higher than the prediction made by the mRP that neglect the interaction between the polymer chains in blends.

These results reveal the significant predictive capability of the RDP (coupling) model, highlighting its ability to distinguish differences between the RDP and mRP models. The coupling effect in the RDP model leads to higher stretch within the contracting region compared to the mRP model, primarily due to the enhanced stretch relaxation captured by the RDP model. The contrasting predictions of both models demonstrate their accuracy in modeling the behaviors and interactions of polymer blends in complex flow conditions. This validates the effectiveness of the RDP (coupling) model in accurately

predicting the complex interactions among polymer species within the blends. On the other hand, neglecting the interaction between the polymer chains, as described by the mRP model, may result in less accurate predictions of the polymer behavior particularly under conditions such as elongational flow that is generated when the flow moves through the converging region of the hyperbolic geometry.

4.1.3. Effect of blend composition

Exploring the blend composition effects by varying the volume fraction of short and the long in the blends helps to enhance the knowledge in understanding polymer behavior. Figure 7 shows the results for the fat tube stretch and thin tube stretch with the 5%, 10% and 20% of long chain species blended with 95%, 90% and 80% of the short species respectively. From Figure 7*a*, the stretch in the fat tube is the highest when $\phi_L = 0.05$ and the lowest when $\phi_L = 0.2$. This means the stretch decreases as ϕ_L increases. As reported in Boudara et al. [2], as the fraction of the long chain decreases, the effective stretch relaxation time along the fat tube increases. This explain the trend in Figure 7*a*.

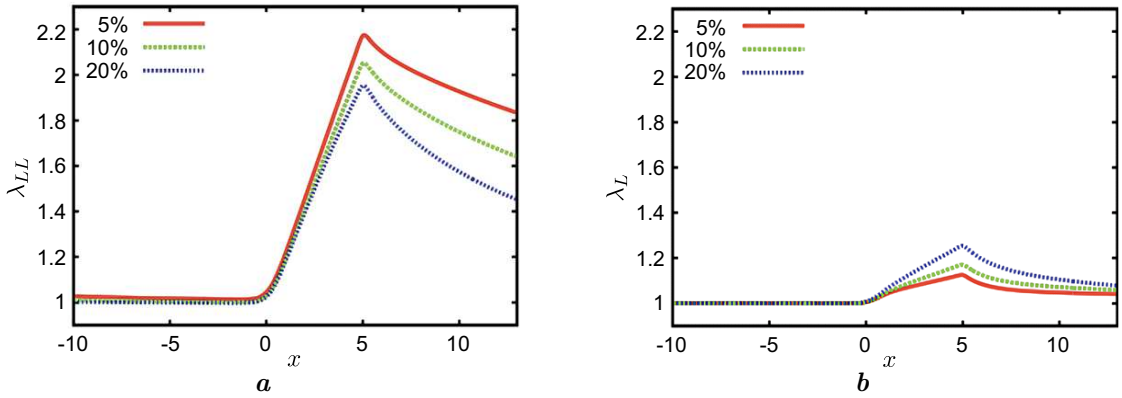

Fig. 7. Centre-line plot of the hyperbolic contraction flow with contraction length, $L = 5$ predicted by bi-disperse RDP model for different blend compositions, 5%, 10% and 20% of the long chain in blends flowing with the same VFR of 4.8. (***a***) Left-hand figure shows the fat-tube stretches. (***b***) Right-hand figure shows the thin tube stretches.

In Figure 7*b*, the opposite trend is observed. The stretch in the thin tube increases as the long chain contribution increases. This is because adding more long-chain components to the blends increases the likelihood of polymer chain entanglement, which restricts movement and promotes alignment along the flow direction, thereby enhancing stretching.

4.2. Cross–slot flow

The cross–slot geometry is another versatile tool and popular choice used to study extensional flow, primarily due to the central stagnation point, where significant fluid stretching occurs, allowing for the analysis of extensional properties such as extensional viscosity. In a cross–slot setup, fluid enters through two opposite inlet arms and exits through two perpendicular outlet arms, as shown in Figure 8. The inlet streams converge at the center of the device, creating a significant elongational flow along the centre-line and generates high-stress stretching at the intersection due to the presence of stagnation point at the centre point of the device.

The hyperbolic corner design promotes a gradual increase in flow velocity, resulting in a uniform extension-rate along the centre-line, which is ideal for studying viscoelastic fluid behavior. While extensional stress dominates along the centre-line, shear stress becomes more pronounced near the channel walls. This geometry provides a unique combination of controlled extensional and shear flows that is suitable for investigating complex fluid behavior. In this research, the aim is to study the stretching behavior of polymeric fluids using the selected constitutive models, the mRP and RDP, and the focus is on examining the behavior along the centre-line, where a pure elongational flow is established.

The hyperbolic corner of the geometry shown in Figure 8 is defined based on the quadrant. With the stagnation point at the origin, the definition is divided into two distinct regions: one for positive

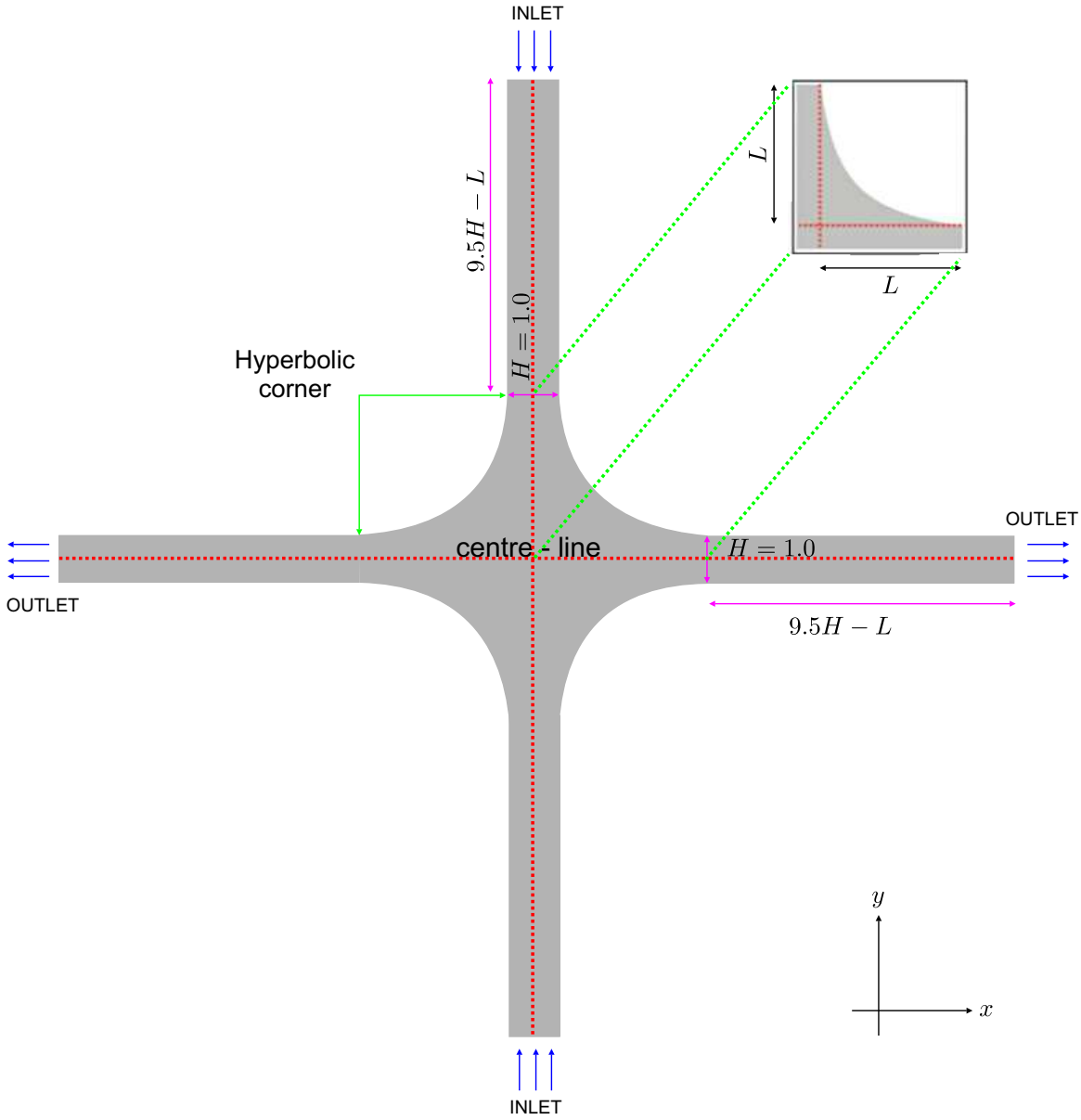

Fig. 8. The geometrical definition for two-dimensional cross-slot with hyperbolic corner and the fluid flow direction. The stagnation point is at the origin of the axes.

y-values and another for negative y-values. For the positive y-value, $y = H(x)$ is defined according to the following piecewise function:

$$H(x) = \begin{cases} 0.5H, & x < -(L+0.5), \\ \frac{-0.5H(L+0.5)}{x}, & -(L+0.5) \leqslant x \leqslant -0.5, \\ \frac{0.5H(L+0.5)}{x}, & 0.5 \leqslant x \leqslant (L+0.5), \\ 0.5H, & x > L + 0.5. \end{cases}$$

On the other hand, for a negative y-axis, $y = -H(x)$, $H(x)$ is defined as

$$H(x) = \begin{cases} -0.5H, & x < -(L+0.5), \\ \frac{0.5H(L+0.5)}{x}, & -(L+0.5) \leqslant x \leqslant -0.5, \\ \frac{-0.5H(L+0.5)}{x}, & 0.5 \leqslant x \leqslant (L+0.5), \\ -0.5H, & x > L + 0.5. \end{cases}$$

Conversely, along the negative y-axis, $y = -H(x)$.

The flow is evolved by the pressure ramping protocol at the inlet and no-slip boundary conditions is set up at the walls, and the stress is linearly extrapolated at the walls by setting up the `linearExtrapolation` utility available in the `rheoTool` toolbox [33] is used to extrapolate the stress at the walls. The influence of geometrical effect, coupling, and blend composition are studied to better understand the extensional behavior of the bi-disperse blends flowing in cross-slot geometry with hyperbolic corners.

4.2.1. Effect of hyperbolic corner length

Geometrical configuration plays an important role in capturing the extensional behavior of the viscoelastic fluid. In this paper, three hyperbolic contraction lengths corners are considered, $L = 2, 3$ and 4. The comparison of the stretch is made against the cross-slot with sharp corner. The inlet pressure for different lengths are adjusted so that the volumetric flow-rate for all simulations are the same for comparable results.

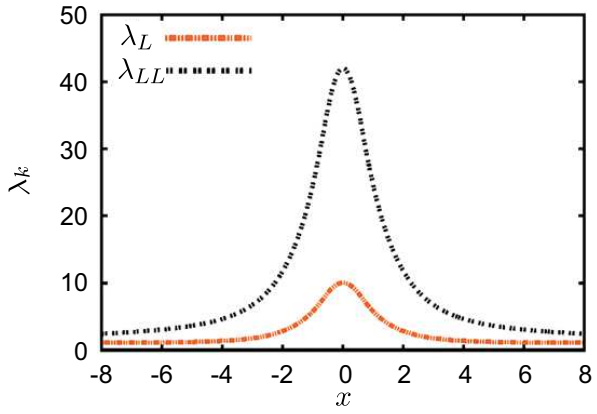

Fig. 9. Centre-line plot for the thin-tube stretch and fat-tube predicted by bi-disperse RDP model for a cross-slot with sharp corner flowing with VFR ≈ 3.65.

Figures 9 and 10 display the centre-line plots for fat and thin tubes stretches near the intersection arms of the cross-slot flow device, featuring both sharp and hyperbolic corners with varying lengths, respectively. The predictions made by the cross-slot show significantly higher value when compared to the hyperbolic corner, leading to a clear separation between the plots for the sharp and hyperbolic corners. As the flow approaches the stagnation point of the sharp corner, it undergoes abrupt changes in direction, which strongly induces an extensional component in the region. The extension-rate, particularly at the stagnation point, is high, leading to a significant increase in the

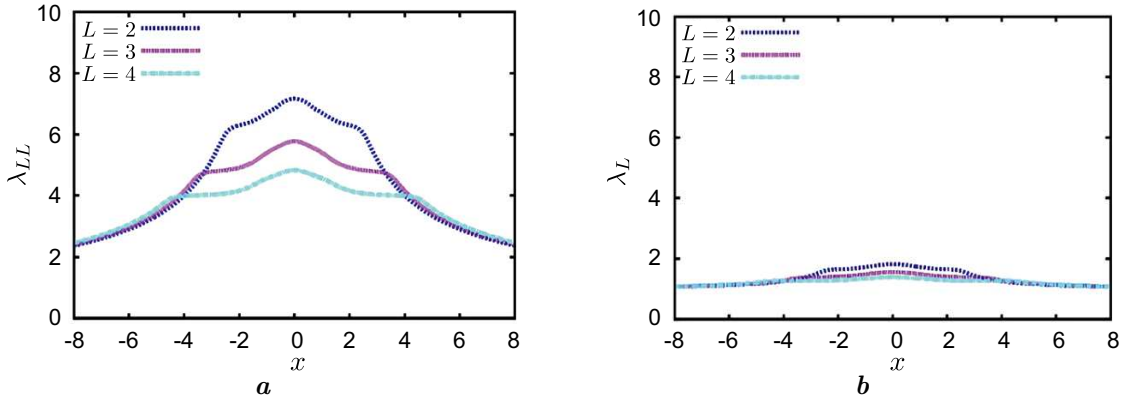

Fig. 10. Centre-line plot for different length of the hyperbolic corner flowing with VFR ≈ 3.65 predicted by bi-disperse RDP model. (***a***) Left-hand figure shows the fat-tube stretches. (***b***) Right-hand figure shows the thin tube stretches.

stretch of the tubes, especially those made of long-chain polymers. Comparing the stretch values for the both tubes, the stretch in the fat tube is approximately four times greater than that in the thin tube.

The extension-rates vary for cross-slot geometries with different hyperbolic corners, ranging from 1.5 to 3 within the hyperbolic region. Given that $\tau_{R,L} = 0.2$, it follows that $\tau_{R,L}\dot{\varepsilon} < 1$. In steady extensional flow, the expected stretch of the thin tube is $\lambda_L = (1 - \tau_{R,L}\dot{\varepsilon})^{-1}$. On the other hand, the stretch of the fat tube is approximately $\phi_L^{-1/2}$ times greater.

To sum up, the geometrical changes significantly influence the velocity gradient (the extension-rate). A cross-slot with sharp corners creates steep velocity gradients due to the rapid acceleration of the

fluid toward the stagnation point. In contrast, a longer hyperbolic corner produces a more moderate velocity gradient because the flow experiences less intense changes and moves gradually through the hyperbolic zone. This implies that the stretches of the thin and fat tubes reduces as the hyperbolic corner length of the cross-slot device increases.

4.2.2. Coupling effect

The effect of coupling between the polymer chains in bi-disperse blends within a cross-slot device having a hyperbolic corner with $L = 2$ can be observed by comparing the coupled RDP model with the equivalent mRP model that shares the same linear rheology. Figure 11 shows the extension-rate with the stretch for the fat tube measured by RDP and mRP models. The predicted extension-rates shown in Figure 11*a* are nearly identical, except at the stagnation point, where the RDP model predicts slightly lower values compared to the mRP model due to higher resistance to stretching flow.

In Figure 11*b*, a significant difference is observed between the predictions of the RDP model and the mRP model. The RDP model predicts a much higher stretch for the interaction between long chains, despite both models experiencing similar extension-rates within the hyperbolic region. Even though the mRP model has a slightly higher extension-rate at the stagnation point compared to the RDP model, the stretch predicted by the RDP model is about three times greater. The difference is due to the enhanced stretch relaxation time in the RDP model, which captures the more complex dynamics of polymer chain relaxation by accounting for interactions between entangled polymer chain interactions that are not fully captured by the mRP model. Additionally, the onset of the fat tube stretch predicted by the RDP model is observed to begin in the upstream region even before the flow accelerates through the hyperbolic corners.

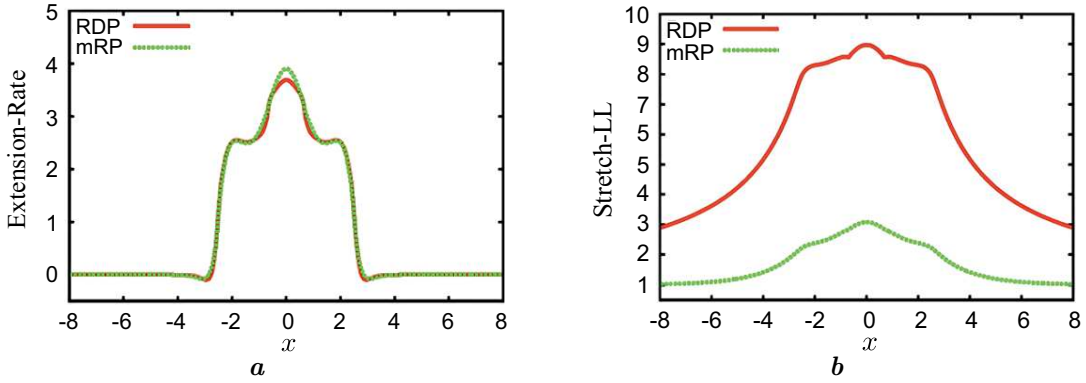

Fig. 11. Centre-line plot for different length of the hyperbolic corner flowing with VFR ≈ 3.65 predicted by bi-disperse RDP model. (***a***) Left-hand figure shows the fat-tube stretches. (***b***) Right-hand figure shows the thin tube stretches.

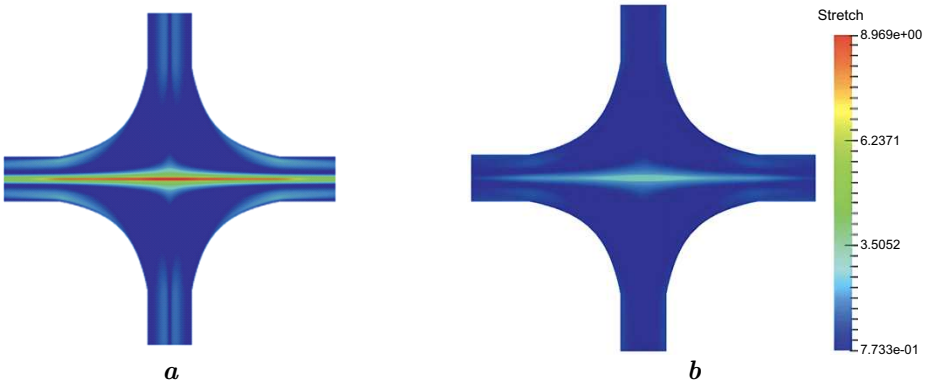

Fig. 12. Fat tube stretch contour of the RDP and mRP at extension-rate, $\dot{\varepsilon} = 2.5$. (***a***) Left-hand figure shows the stretch contour for the fat tube composed only of L-chains, $\lambda_{LL} = \sqrt{\operatorname{tr} A_{LL}/3}$ predicted by RDP model. (***b***) Right-hand figure shows the stretch contour of the first mode (with the longest relaxation time) predicted by uncoupled mRP model.

Figure 12 shows color contours captured near the centre of the device, including the four arms. The contours are plotted with the same extension-rate along the centre-line as shown in Figure 11*a*. Throughout the domain in Figure 12, it is evident that no significant stretch is observed in the inlet arms for either model, particularly in the predictions made by the mRP model. The fluid accelerates toward the opposite direction of the outlet arms, creating elongational flow along the horizontal centre-line.

This flow elongates the stretching component of the fluid near the neighbouring stagnation point and reaches a maximum at the stagnation point. The stretching component is observed to gradually diminish as the fluid flows into the downstream region.

4.2.3. Effect of blend composition

Bi-disperse polymer blends demonstrate the complex extensional rheology as a result of the interactions between the polymer chains with different molecular weights. Investigating the impact of various polymer chain lengths in these blends is crucial for understanding flow behavior, particularly under stretching conditions. Utilizing a cross-slot device is a valuable method for studying the behavior of these blends under near-pure elongational flow conditions at the centre-line.

Three different blends are examined to study the influence of blend composition on elongational flow along the horizontal outlet centre-line. In each case, pressure drops are adjusted to achieve the same volumetric flow rate for comparison purposes. Figure 13 shows the centre-line plots for blends with 5%, 10%, and 20% long polymer chain contributions. Within the hyperbolic corner, the extension-rate loses its uniformity for the 20% long chain polymer. This occurs because a higher concentration of long polymer chains leads to greater modification of the flow, resulting in enhanced resistance to extensional flow.

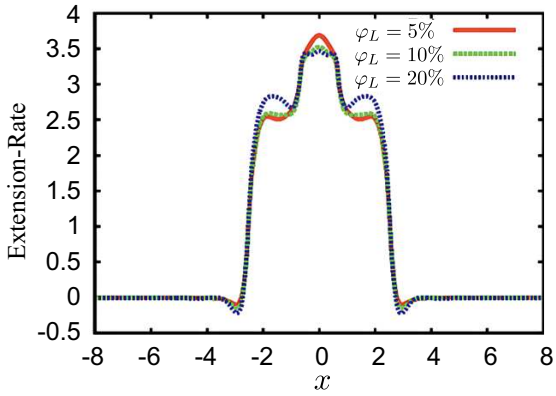

Fig. 13. Centre-line plot of the cross-slot with hyperbolic corner ($L = 2$) for extension-rate predicted by bi-disperse RDP model for different blend compositions flowing with the same VFR of 4.8.

Figure 14 shows the stretching behavior of the fat and thin tubes at the horizontal outlet centre-line for different concentration of the long chain polymer flowing with the same volumetric flow rate. The RDP model predicts demonstrate the opposite trend of the stretch for the thin and fat tubes along with the increment of the long polymer chains in the blend.

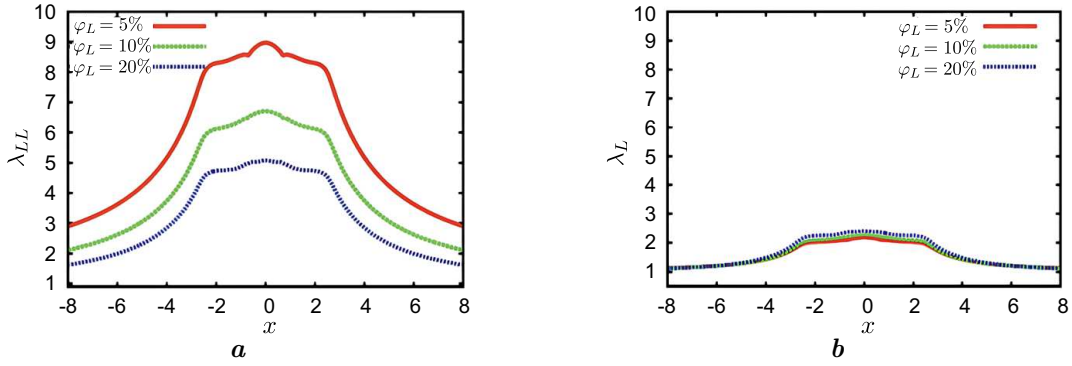

Fig. 14. Centre-line plot for different blend composition flowing with VFR ≈ 4.8 predicted by bi-disperse RDP model. (***a***) Left-hand figure shows the fat-tube stretches. (***b***) Right-hand figure shows the thin tube stretches.

The fat tube stretch decreases as the long chain concentration increases. This is because, as the long chain contribution increases, the effective stretch relaxation time increases as noted in Boudara et al. [2]. A longer relaxation time means the polymer will experience a greater resistance to stretching and

restrict the ability of the polymer to stretch effectively. In contrast, the thin tube stretch is increases with the increment of the long chain concentration. The higher density of long chains enhances the likelihood of these chains becoming entangled with each other and increases the proportion of long chain entanglements, which more than compensates for the reduced stretchability of this portion.

4.3. Hyperbolic contraction flow versus cross–slot flow

This section presents the comparison between two geometrical flows discussed in the previous section. While the hyperbolic contraction geometry is flowing in one-dimensional, the cross-slot geometry with hyperbolic corners is flowing in two-dimensional. For a comparable result, the extension-rate for both flows within the hyperbolic region were adjusted to give the same extension-rate that is $\dot{\varepsilon} = 2.5$. The hyperbolic contraction length for the corner of Cross–Slot Flow (CSF) is set to $L = 2$ and contraction length, $L = 5$ for Hyperbolic Contraction Flow (HCF) as these give equivalent distance of the extensional flow created along the geometrical centre-line of the contraction region for both devices.

Chain stretch in the cross–slot flow. Figure 15 shows the chain stretch for the fat tube and thin tube with the maximum extension-rate along the centre-line is about 2.5 in both geometrical flow. It is worth noting that, the value $X = 0$ from Figure 15 marks the onset of the contraction for the HCF whereas in CSF it represents the centre of geometry where the stagnation point is located. Figure 15*a* reveals the stretch within the tube that form by the entanglement of the same species for the long chains (that is sometimes called the fat tube), $\lambda_{LL} = \sqrt{\operatorname{tr} \mathbf{A}_{LL}/3}$. It is pronounced from the figure that the stretch for the tube made up by entirely long chain shows a significant increase of stretch as a consequence of the enhanced stretch relaxation effect that is captured by the RDP model. Compared to Figure 15*b*, the blends is dominated by 95% short-chain and only 5% of the long chain, thus the stretch in a thin tube that shows a slight stretch of the melt within the contraction region. This trend shows the same in both devices as expected.

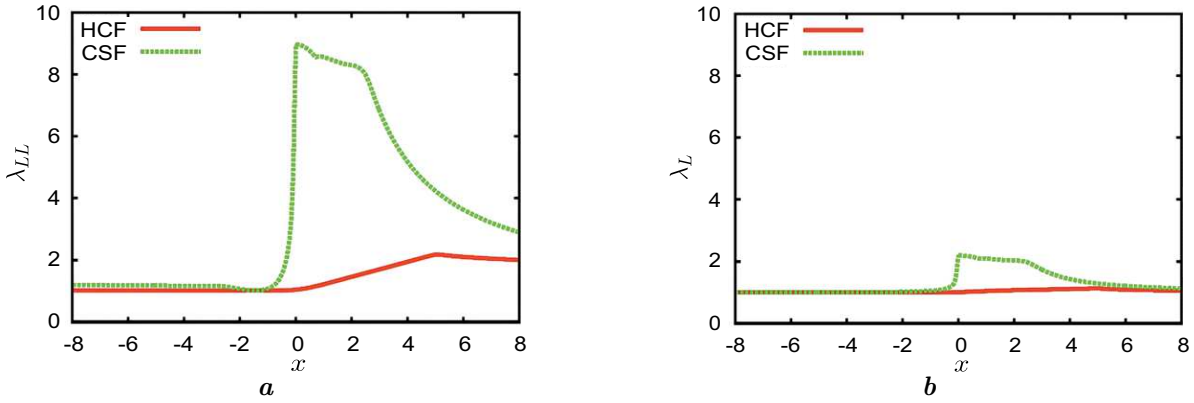

Fig. 15. Graphs showing the extension of the L-chain component along the centre-line of the 4:1 hyperbolic contraction flow and cross-slot flow for the RDP model. (***a***) Left-hand figure shows the stretch in the fat tube composed only of L-chains, $\lambda_{LL} = \sqrt{\operatorname{tr} A_{LL}/3}$. (***b***) Right-hand figure shows the stretch in the thin tube composed only of L and S chains, $\lambda_L = \sqrt{\operatorname{tr} A_L/3}$.

Comparing the stretches in both tubes and both geometrical flows, it is observed that a rapid increase of the stretches is captured by the cross-slot flow approaching the stagnation point gives the maximum stretch at the stagnation point, and relaxes downstream. This is primarily due to the nature of the CSF, where the stagnation point is centrally located within the geometry, ensuring that the surrounding residence time is adequate to achieve equilibrium stretch. However, in HCF, the transient growth of stretch is observed. It is worth reemphasizing that the main difference that distinguishes the two flows is the presence of the stagnation point at the center of the cross slot which significantly affects the residence time of the melt. This explains the reason for the difference in transit time of the flowing polymer in the two devices.

5. Conclusion

Understanding the behavior of the bi-disperse blend through one-dimensional and two-dimensional through the hyperbolic contraction and cross-slot geometry provides valuable insight into the extensional response of the bi-disperse polymer that can be captured by the new constitutive model introduced by Boudara et al. [2], the RDP model which was developed to describe a more realistic description of the polydispersity capturing the complex behavior effectively. This work focuses on the interaction of the polymer blend composed of two different molecular weights, simplifying the model to 2 components which requires 4 modes to be computed in each computational cell and time step.

In this paper, the results reveal that the RDP model predicts a higher stretch of the long chain component compared to the mRP model, even though both models share the same linear rheology. This is due to the enhanced stretch relaxation time in the RDP model, which allows for significant stretching at the stagnation point of the device because of the increment of the residence time in that region. In contrast, the mRP model lacks a detailed representation of entanglement dynamics, leading to an underestimation of the stretching effect. Therefore, The RDP model provides more reliable predictions than the mRP model due to its inclusion of interactions between all modes, a feature absent in the mRP formulation. During the melting process of a polymer blend, physical and molecular transformations occur, including interactions between polymer chains of different molecular weights. The RDP model accounts for these interactions through its constitutive equations, while the mRP model does not. Consequently, the predictions of the RDP model are expected to more accurately reflect the realistic behavior of polymer blends compared to those of the mRP model. The effect of the blend composition shows opposite trends in the stretch predicted by the fat and thin tube as the concentration of the blends of the long chains increases in both devices.

Comparing the two geometrical flows in section 4.3, the CSF is more effective in capturing the extensional fluid properties which make it a valuable tool in numerical simulations studies and experiments to investigate the phenomena such as flow instabilities and the stretching effects of the polymer melts under complex flow conditions. The existence of the stagnation point at the centre of the cross-slot device enhances the stretching behavior due to strong extensional flow generated near the stagnation point.

Exploring higher coupling modes between polymer chains presents an interesting direction for future work. However, extending the model to more complex polydisperse systems would require solving N^2 coupling equations, leading to significant computational demands. To mitigate this, potential strategies include employing parallel computing and adaptive meshing within the computational domain to enhance efficiency and reduce computational costs.

[1] Maxwell J. C. IV. On the dynamical theory of gases. Philosophical Transactions of the Royal Society of London. **157**, 49–88 (1867).

[2] Boudara V. A., Peterson J. D., Leal L. G., Read D. J. Nonlinear rheology of polydisperse blends of entangled linear polymers: Rolie-Double-Poly models. Journal of Rheology. **63** (1), 71–91 (2019).

[3] Graham R. S., Likhtman A. E., McLeish T. C. B., Milner S. M. Microscopic theory of linear, entangled polymer chains under rapid deformation including chain stretch and convective constraint release. Journal of Rheology. **47** (5), 1171–1200 (2003).

[4] De Gennes P. G. Reptation of a polymer chain in the presence of fixed obstacles. The Journal of Chemical Physics. **55** (2), 572–579 (1971).

[5] Doi M., Edwards S. F., Edwards S. F. The theory of polymer dynamics. Oxford University Press. Vol. 73 (1988).

[6] Auhl D., Ramirez J., Likthman A. E., Chambon P., Fernyhough C. Linear and nonlinear shear flow behavior of monodisperse polyisoprene melts with a large range of molecular weights. Journal of Rheology. **52** (3), 801–835 (2008).

[7] Taghipour H., Salvatore C., Dimitris V., Evelyne V. R., Laurence G. D. H. Entangled linear polymers in fast shear flows: Comparison of tube-model predictions and experimental data. Journal of Rheology. **65** (6), 572–579 (2021).

[8] Anwar M., Graham R. S. Nonlinear shear of entangled polymers from nonequilibrium molecular dynamics. Journal of Polymer Science Part B: Polymer Physics. **57** (24), 1692–1704 (2019).

[9] Tezel A. K., Oberhauser J. P., Graham R. S., Jagannathan K., McLeish T. C., Leal L. G. The nonlinear response of entangled star polymers to startup of shear flow. Journal of Rheology. **53** (5), 1193–1214 (2009).

[10] Likhtman A. E., Graham R. S. Simple constitutive equation for linear polymer melts derived from molecular theory: Rolie–Poly equation. Journal of Non-Newtonian Fluid Mechanics. **114** (1), 1–12 (2003).

[11] Lord T. D., Scelsi L., Hassell D. G., Mackley M. R., Embery J., Auhl D., Harlen O. G., Tenchev R., Jimack P. K., Walkley M. A. The matching of 3D Rolie-Poly viscoelastic numerical simulations with experimental polymer melt flow within a slit and a cross-slot geometry. Journal of Rheology. **54** (2), 355–373 (2010).

[12] Collis M. W., Lele A. K., Mackley M. R., Graham R. S., Groves D. J., Likhtman A. E., Nicholson T. M., Harlen O. G., McLeish T. C. B., Hutchings L. R., Fernyhough C. M., Young R. N. Constriction flows of monodisperse linear entangled polymers: Multiscale modeling and flow visualization. Journal of Rheology. **49** (2), 501–522 (2005).

[13] Taghipour H., Hawke L. G. Entangled linear polymers in fast shear and extensional flows: evaluating the performance of the Rolie–Poly model. Rheologica Acta. **60** (10), 617–641 (2021).

[14] Peterson J. D., Cromer M., Fredrickson G. H., Gary Leal L. Shear banding predictions for the two-fluid Rolie–Poly model. Journal of Rheology. **60** (5), 927–951 (2016).

[15] Reis T., Wilson H. J. Rolie–Poly fluid flowing through constrictions: Two distinct instabilities. Journal of Non-Newtonian Fluid Mechanics. **195**, 77–87 (2013).

[16] Adams J. M., Fielding S. M., Olmsted P. D. Transient shear banding in entangled polymers: A study using the Rolie–Poly model. Journal of Rheology. **55** (5), 1007–1032 (2011).

[17] Des Cloizeaux J. Double reptation vs. simple reptation in polymer melts. Europhysics Letters. **5** (5), 437 (1988).

[18] Nystrom M., Tamaddon Jahromi H. R., Stading M., Webster M. F. Numerical simulations of Boger fluids through different contraction configurations for the development of a measuring system for extensional viscosity. Rheologica Acta. **51**, 713–727 (2012).

[19] Cogswell F. N. Converging flow and stretching flow: a compilation. Journal of Non-Newtonian Fluid Mechanics. **4** (1–2), 23–38 (1978).

[20] Nyström M., Tamaddon Jahromi H. R., Stading M., Webster M. F. Hyperbolic contraction measuring systems for extensional flow. Mechanics of Time-Dependent Materials. **21**, 455–479 (2017).

[21] Kim H. C., Pendse A., Collier J. R. Polymer melt lubricated elongational flow. Journal of Rheology. **38**, (4) 831–845 (1994).

[22] Collier J. R., Romanoschi O., Petrovan S. Elongational rheology of polymer melts and solutions. Journal of Applied Polymer Science. **69** (12), 2357–2367 (1998).

[23] Cruz F. A., Poole R. J., Afonso A. M., Pinho F. T., Oliveira P. J., Alves M. A. A new viscoelastic benchmark flow: Stationary bifurcation in a cross-slot. Journal of Non-Newtonian Fluid Mechanics. **214**, 57–68 (2014).

[24] Kordalis A., Varchanis S., Ioannou G., Dimakopoulos Y., Tsamopoulos J. Investigation of the extensional properties of elasto-visco-plastic materials in cross-slot geometries. Journal of Non-Newtonian Fluid Mechanics. **296**, 104627 (2021).

[25] Davoodi M., Domingues A. F., Poole R. J. Control of a purely elastic symmetry-breaking flow instability in cross-slot geometries. Journal of Fluid Mechanics. **881**, 1123–1157 (2019).

[26] Poole R. J., Rocha G. N., Oliveira P. J. A symmetry-breaking inertial bifurcation in a cross-slot flow. Computers & Fluids. **93**, 91–99 (2014).

[27] Rocha G. N., Poole R. J., Alves M. A., Oliveira P. J. On extensibility effects in the cross-slot flow bifurcation. Journal of Non-Newtonian Fluid Mechanics. **156** (1–2), 58–69 (2019).

[28] Hassell D. G., Mackley M. R. An experimental evaluation of the behavior of mono and polydisperse polystyrenes in cross-slot flow. Rheologica Acta. **48**, 543–550 (2009).

[29] Read D. J., Jagannathan K., Sukumaran S. K., Auhl D. A full-chain constitutive model for bidisperse blends of linear polymers. Journal of Rheology. **56** (4), 823–873 (2012).

[30] Auhl D., Chambon P., McLeish T. C., Read D. J. Elongational flow of blends of long and short polymers: Effective stretch relaxation time. Physical Review Letters. **103** (13), 136001 (2009).

[31] Weller H. G., Tabor G., Jasak H., Fureby C. A tensorial approach to computational continuum mechanics using object-oriented techniques. Computers in Physics. **12** (6), 620–631 (1998).

[32] Favero J. L., Secchi A. R., Cardozo N. S. M., Jasak H. Viscoelastic flow simulation: development of a methodology of analysis using the software OpenFOAM and differential constitutive equations. Computer Aided Chemical Engineering. **27**, 915–920 (2009).

[33] Pimenta F., Alves M. A. Stabilization of an open-source finite-volume solver for viscoelastic fluid flows. Journal of Non-Newtonian Fluid Mechanics. **239**, 85–104 (2017).

[34] Van Doormaal J. P., Raithby G. D. Enhancements of the SIMPLE method for predicting incompressible fluid flows. Numerical Heat Transfer. **7** (2), 147–163 (1984).

[35] Tenchev R., Gough T., Harlen O. G., Jimack P. K., Klein D. H., Walkley M. A. Three-dimensional finite element analysis of the flow of polymer melts. Journal of Non-Newtonian Fluid Mechanics. **166** (5–6), 307–320 (2011).

Чисельне моделювання течії бідисперсних полімерів у складних геометріях з використанням моделі Rolie–Double–Poly у програмному забезпеченні OpenFOAM

Азахар А. А.[1], Олівер Г. Х.[2], Марк А. В.[3], Рамлі Н.[1]

[1] *Школа математичних наук, Університет науки Малайзії, 11800 USM, Пенанг, Малайзія*
[2] *Школа математики, Університет Лідса, LS2 9JT, Великобританія*
[3] *Школа обчислювальної техніки, Університет Лідса, LS2 9JT, Великобританія*

Моделювання поведінки бідисперсних, лінійно переплетених полімерних сумішей за допомогою конститутивного рівняння Rolie–Double–Poly має важливе значення для розуміння надійності моделі при моделюванні поведінки складних потоків. У цій статті досліджується реакція на розтягування полімерних сумішей, зокрема розтягнення ланцюгів під дією чистого розтягувального потоку вздовж центральної лінії в двох геометріях потоку: гіперболічний скорочувальний потік і поперечний потік з гіперболічними кутами. Зв'язані та незв'язані моделі були реалізовані в програмному забезпеченні OpenFOAM за допомогою набору інструментів `RheoTool`, де моделювання використовує вирішувач `rheoFoam` для моделювання потоку нестисливої в'язкопружної рідини. Ефект, включаючи довжину скорочення, склад суміші довжин ланцюга та зв'язок ланцюга, є ключовими факторами в цьому дослідженні. Один із важливих результатів показує, що модель Rolie–Double–Poly точніше фіксує поведінку розтягування полімерних ланцюгів порівняно з незв'язаною моделлю, підкреслюючи її потенційну застосовність для складнsіих полідисперсних систем.

Ключові слова: *Rolie–Double–Poly; Rolie–Poly; гіперболічний скорочувальний потік; перехресний потік; OpenFOAM; RheoTool.*